Numerical Simulation of Heavy Particle Dispersion—Scale Ratio and Flow Decay Considerations

Lian-Ping Wang[1]

David E. Stock

Department of Mechanical & Materials Engineering, Washington State University, Pullman, WA 99164-2920

Lagrangian statistical quantities related to the dispersion of heavy particles were studied numerically by following particle trajectories in a random flow generated by Fourier modes. An experimental fluid velocity correlation was incorporated into the flow. Numerical simulation was performed with the use of nonlinear drag. The simulation results for glass beads in a nondecaying turbulent air showed a difference between the horizontal dispersion coefficient and vertical dispersion coefficient. This difference was related to the differences of both the velocity scale and the time scale between the two direction. It was shown that for relatively small particle sizes the particle time scale ratio dominates the value of the diffusivity ratio. For large particles, the velocity scale ratio reaches a value of $1/\sqrt{2}$ and thus fully determines the diffusivity ratio. Qualitative explanation was provided to support the numerical findings. The dispersion data for heavy particles in grid-generated turbulences were successfully predicted by the simulation when flow decay was considered. As a result of the reduction in effective inertia and the increase in effective drift caused by the flow decay, the particle dispersion coefficient in decaying flow decreases with downstream location. The particle rms fluctuation velocity has a slower decay rate than the fluid rms velocity if the drift parameter is large. It was also found that the drift may substantially reduce the particle rms velocity.

1 Introduction

Heavy particles are any small passive particles in the flow with a density much larger than the density of the fluid. Heavy particles have a free fall velocity that is of the order of the fluid rms velocity. We are interested in the dispersion process of heavy particles when suspended in and driven by turbulent flows. A knowledge of heavy particle dispersion is beneficial for improving energy conversion and reducing pollution. Lagrangian statistical quantities, calculated by following the random motion of a solid particle, are needed to understand the dispersion process, but they are difficult to obtain experimentally. However, numerical simulation can provide this information by tracking particles through a simulated turbulent flow. Since numerical simulation has a different set of limitations than a theoretical analysis, it can sometimes be used to test the applicability of analytical results. In this paper, we report on the results of a simulation of particle dispersion. Particular attention is paid to ratio of horizontal to vertical scales and effect of flow decay.

We consider the dispersion of heavy particles by turbulence, assuming the particulate phase mass loading is low and, therefore, the particles do not alter the flow. Earlier analytical approaches (Yudine, 1959; Csanady, 1963; Meek and Jones, 1973) have shown that the drift velocity of a particle due to an external body force greatly reduces the particle dispersion. The drift is also found to cause nonisotropic dispersion. Particles disperse more in the direction parallel to the drift velocity (the vertical direction) than in the directions normal to the drift (the horizontal directions). This is known as the continuity effect (Csanady, 1963). Reeks (1977), Pismen and Nir (1978), Nir and Pismen (1979) have simultaneously considered the effect of the particle inertia and the drift on the dispersion. However, their work has been limited to small particles for which Stokes' drag force applies, and to homogeneous, isotropic turbulence.

Particle dispersion in grid-generated turbulence has been experimentally measured by Snyder and Lumley (1971), Wells and Stock (1983), and Ferguson (1986). The experimental work qualitatively confirms the theoretical predictions. The grid-generated turbulence, while being the simplest experimental turbulent flow, is not homogeneous in the mean flow direction, since the turbulence decays due to viscous dissipation. Approximate quantitative comparison between the experimental data and the analytical predictions is possible by making a quasi-stationarity assumption (Nir and Pismen, 1979). Particle dispersion can also be predicted by direct numerical simulation (Riley and Paterson, 1974; Ueda et al., 1983, and Squires and Eaton, 1990), but this method is prohibitively time consuming and is limited to flows of low Reynolds numbers.

Kraichnan's method (1970) for simulating turbulence using Fourier modes is physically sound and computationally efficient. It is especially useful for particle dispersion studies since a large number of particle trajectories have to be computed.

[1] Current Address: Department of Mechanical Engineering, Pennsylvania State University, University Park, PA 16802.

Contributed by the Fluids Engineering Division for publication in the JOURNAL OF FLUIDS ENGINEERING. Manuscript received by the Fluids Engineering Division February 7, 1992; revised manuscript received March 18, 1993. Associate Technical Editor: M. W. Reeks.

This turbulence-simulation method has been used to test the analytical results of particle dispersion obtained by Eulerian direct interaction (Reeks, 1980) and to study the effect of Basset history force on particle dispersion (Reeks and McKee, 1984). The same model was used by Ferguson (1986) to simulate the effect of fluid continuity on heavy particle dispersion and by Maxey (1987) to calculate the average settling velocity of particles in a turbulent flow. Turfus and Hunt (1986) extended the model to inhomogeneous turbulence by adding an irrotational velocity field. The model has the potential to include the advection of small eddies by large eddies (Fung et al., 1992). Recently, Ounis and Ahmadi (1989) employed Kraichnan's model to study the relative importance of various forces acting on a solid particle and to find Lagrangian velocity moments. Wang and Stock (1992) studied the effect of nonlinear drag on the particle dispersion using the same numerical simulation techniques. They found that the nonlinear drag must be considered when calculating particle dispersion if the ratio of the drift velocity to the fluid rms fluctuating velocity is greater than two. They also compared the results of numerical simulations to those of an analytical calculation based on the second order iteration technique (Reeks, 1977). Among these studies, only Ounis and Ahmadi (1989) tried to compare the simulation results with experimental data.

The purpose of this study was to use numerical simulations based on Kraichnan's method to help us understand experimental data for heavy particle dispersion in the grid-generated turbulent flow (i.e., the data of Snyder and Lumley, 1971; Wells and Stock, 1983; and Ferguson, 1986). Particular attention was paid to the following two questions: 1) How does the diffusivity ratio (the ratio of particle dispersion coefficient in the horizontal direction to that in the vertical direction) change with particle size for glass beads in typical wind tunnel turbulence and how is the diffusivity ratio related to the velocity scale ratio and the integral time scale ratio? 2) What is the effect of the flow decay on the dispersion of heavy particles? The answer to the first question will help clarify the results of Ferguson (1986). The answer to the second question will allow us to compare the simulation results with the experimental data.

The paper is organized as follows. First, Kraichnan's model of turbulence generation is extended to allow various fluid velocity correlations to be used. Some programming techniques necessary for large drift velocity are then discussed. The results of numerical simulation for long-time dispersion statistics for glass beads in nondecaying turbulence are reported in Section 4. In Section 5, flow decay is considered and comparisons are made between the simulation results and the experimental data (Synder and Lumley, 1971; and Wells and Stock, 1983).

2 Structure of Simulated Turbulence

The flow field was represented by the following equation which is a linear superposition of a large number of Fourier modes with random amplitudes and phases (Kraichnan, 1970)

$$u_i(x_i,t)/u_0=\sum_{n=1}^{N}\{b_i^{(n)}\cos(k^{(n)}\cdot x+\omega^{(n)}t) + c_i^{(n)}\sin(k^{(n)}\cdot x+\omega^{(n)}t)\}. \quad (1)$$

Here N is the number of Fourier modes and u_0 is the rms fluctuation velocity. The mean velocity is zero, and the velocity field is understood to represent the velocity field in a frame of reference moving with the mean velocity of the flow (moving Eulerian frame or mE). For each n, values of $k_1^{(n)}$, $k_2^{(n)}$, $k_3^{(n)}$, and $\omega^{(n)}$ are chosen independently with probability density functions (pdf) $P_{11}(k_1)$, $P_{12}(k_2)$, $P_{13}(k_3)$ and $P_2(\omega)$, respectively. Real coefficients $b_i^{(n)}$ and $c_i^{(n)}$ are independent Gaussian random variables which have been filtered such that $b^{(n)}\cdot k^{(n)}$ and $c^{(n)}\cdot k^{(n)}$ vanish, to make the overall flow field incompressible. The ensemble averaged two-point correlation for this random flow field is (Maxey, 1987)

$$R_{ij}(r,\tau)/u_0^2=N\int_{-\infty}^{\infty}d^3k\int_{-\infty}^{\infty}d\omega \times P_{11}(k_1)P_{12}(k_2)P_{13}(k_3)P_2(\omega)\Gamma^2(k_1,k_2,k_3,\omega) \times\left[\delta_{ij}-\frac{k_ik_j}{k^2}\right]\cos(k\cdot r+\omega\tau). \quad (2)$$

where $\Gamma(k_1, k_2, k_3, \omega)$ is the scaling function.

Nomenclature

b_i, c_i = random coefficients
d_p = diameter of particle
$D(\tau)$ = one-point fluid velocity correlation in the moving Eulerian frame
$E(k)$ = scalar energy spectrum function
f = ratio of drag coefficient to Stokes drag
$f(r)$ = fluid longitudinal spatial velocity correlations
$g(r)$ = fluid transverse spatial velocity correlation
$F(\omega)$ = frequency spectrum
q = external body force acting on particle
k = wave number
k_0 = characteristic wave number
L_f = integral length scale of $f(r)$
M = grid spacing
N = number of Fourier modes
$P_{1i}(k_i)$ = probability density function of k_i
$P_2(\omega)$ = probability density function of ω
r = space separation
$R_{ij}(r,\tau)$ = fluid velocity correlation
Re_p = particle Reynolds number
St = Stokes number
t = time
T = integral time scale
u = flow velocity
u_0 = fluid rms fluctuation velocity
U = mean flow velocity
v = particle velocity
v_{i0} = particle rms fluctuation velocity
v_d = particle Stokes velocity = $\tau_a q$
v_{d0} = particle drift velocity in still fluid
x = Eulerian coordinate
x_0 = virtual origin of the grid-generated turbulence
y = particle's location
$\alpha(k_i)$ = see Eq. (4)
$\beta(\omega)$ = see Eq. (5)
δ_{ij} = Kronecker delta
ϵ_{ij}^p = particle dispersion coefficient tensor
γ = v_d/u_0
Γ = scaling function
μ = fluid viscosity
ρ = fluid density
ρ_p = particle density
τ = time delay
τ_a = particle aerodynamic response time
ω = frequency
ω_0 = characteristic frequency

Superscripts

(j) = jth mode

Subscripts

1 or 11 = horizontal direction
3 or 33 = vertical direction
fE = fixed Eulerian
i = ith component
L = Lagrangian
mE = moving Eulerian

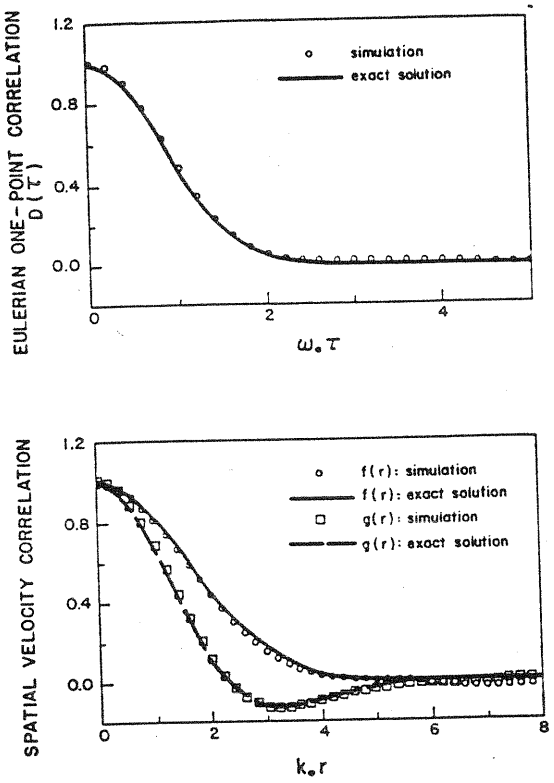

Fig. 1 Velocity correlations computed from the simulated turbulence with finite-modes ($N=80$), compared to the exact forms in Case I. 1800 realizations are used.

For homogeneous isotropic turbulence, the flow structure can be represented by the two functions, $D(\tau)$ and $E(k)$, (Wang and Stock, 1988). $D(\tau)$ is the one point velocity correlation and $E(k)$ is the scalar energy spectrum. For the sake of simplicity, the scaling function is assumed to have the following form,

$$N\Gamma^2(k_i,\omega)=\alpha(k_i)\beta(\omega). \tag{3}$$

Further, the product of $\alpha(k_i)P_{11}(k_1)P_{12}(k_2)P_{13}(k_3)$ is chosen (this can always be done) to be a function of k only, where $k=\sqrt{(k_1^2+k_2^2+k_3^2)}$. Then the spatial energy spectrum is determined by $\alpha(k_i)$ and pdf's of wave number $k_i^{(n)}$ as

$$E(k)=4\pi u_0^2 k^2 P_{11}(k_1)P_{12}(k_2)P_{13}(k_3)\alpha(k_i). \tag{4}$$

The frequency spectrum (the Fourier transform of $D(\tau)$) is related to $\beta(\omega)$ and the pdf of $\omega^{(n)}$ by

$$F(\omega)\equiv\frac{1}{\pi}\int_0^\infty D(\tau)\cos(\omega\tau)d\tau=\beta(\omega)P_2(\omega). \tag{5}$$

The flow structure is prescribed by giving $E(k)$ and $D(\tau)$ and the scaling function Γ is specified as

$$\Gamma^2(k_i,\omega)=\frac{1}{N}\frac{E(k)}{4\pi u_0^2 k^2 P_{11}(k_1)P_{12}(k_2)P_{13}(k_3)}\frac{F(\omega)}{P_2(\omega)}. \tag{6}$$

In other words, the scaling function Γ can be adjusted, according to the probability density functions of random numbers, to produce the proper Eulerian flow statistics. The choice for the pdf functions is not unique but is made to ensure a rapid convergence of fluid velocity correlations (or spectrum functions) for the simulated turbulence.

In all the previous papers (Maxey, 1987; Ferguson, 1986; Ounis and Ahmadi, Wang and Stock, 1992), the pdf functions are assumed to be Gaussian distributions with the scaling function Γ of the form

$$\Gamma(k_1,k_2,k_3,\omega)=\frac{k}{\sqrt{2N}k_0}. \tag{7}$$

It follows that the spectrum function and the correlation function are

$$E(k)=\frac{u_0^2}{\sqrt{2\pi}}\frac{k^4}{k_0^5}\exp\left(-\frac{k^2}{2k_0^2}\right). \tag{8}$$

$$D(\tau)=\exp(-\omega_0^2\tau^2/2). \tag{9}$$

The random velocity field with this structure will be referred to as Case I turbulence. The longitudinal and transverse fluid spatial velocity correlations, $f(r)$ and $g(r)$, can be derived from (8) and are

$$f(r)=\exp(-k_0^2r^2/2), \tag{10a}$$

$$g(r)=(1-k_0^2r^2/2)\exp(-k_0^2r^2/2). \tag{10b}$$

In the simulation, a finite number of Fourier modes, N, was used for one realization of the flow. A separate flow realization was used to calculate each particle trajectory.

The fluid velocity correlations can be accurately reproduced by the simulated turbulence. Figure 1 shows the velocity correlations calculated from the simulated flow by averaging over 1800 flow realizations with $N=80$ for each realization. They all compare well to their exact forms.

The structure of many real turbulent flows is not described by Eqs. (8) and (9). Theoretically, the above simulation method can be used to generate flow fields with any turbulence structure functions by choosing proper pdf functions for the random numbers and proper scaling function. To show this and test how the shape of the correlation curves may affect particle dispersion, we introduce the following forms for the energy spectrum and the one-point Eulerian velocity correlation,

$$E(k)=\frac{3u_0^2}{2\pi}\frac{k^4}{k_0^5[1+k^2/(4k_0^2)]^4}, \tag{11}$$

$$D(\tau)=\cos(\omega_0\tau)\exp(-\omega_0\tau) \tag{12}$$

We will refer to the random velocity field with such a spectrum and correlation function as Case II turbulence. Consequently, the spatial velocity correlations are

$$f(r)=(1+2k_0r)\exp(-2k_0r), \tag{13a}$$

$$g(r)=(1+2k_0r-2k_0^2r^2)\exp(-2k_0r). \tag{13b}$$

The above forms of the temporal and the spatial velocity correlations have appeared in the literature (Townsend, 1976; Calabrese and Middleman, 1979; and Gouesbet et al., 1984).

To generate Case II turbulence, we need to select the proper pdf functions, $P_1i(k_i)$ and $P_2(\omega)$. When Gaussian distributions were used, the velocity correlations of the simulated flow were found to converge very slowly to the prescribed forms. The convergence was slow because the resulting scaling function was extremely large for large wave numbers (or frequencies), thus, the large wave numbers can not be quickly realized in the simulation. To avoid this, we used the Cauchy distributions,

$$P_{1i}(k_i)=\frac{1}{\pi k_0\left[1+\dfrac{k_i^2}{k_0^2}\right]} \tag{14a}$$

$$P_2(\omega)=\frac{1}{\pi\omega_0\left[1+\dfrac{\omega^2}{\omega_0^2}\right]}. \tag{14b}$$

Figure 2 shows the comparison between the velocity correlations obtained directly from the simulated flow and the exact forms. The comparison is satisfactory when 1800 realizations of 80 Fourier modes were used.

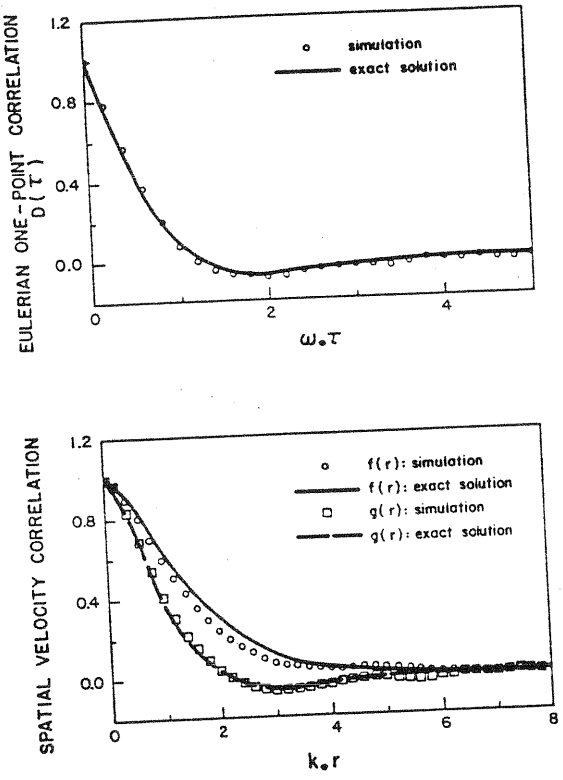

Fig. 2 Velocity correlations computed from the simulated turbulence with finite-modes ($N=80$), compared to the exact forms in Case II. 1800 realizations are used.

Comparing Case I turbulence and Case II turbulence, we find both spectrum functions, (8) and (11), achieve their maximum values at $k=2k_0$, but (11) has a relatively larger fraction of turbulence energy in the higher wave number portion. The integral length scales for $f(r)$ are: $L_f=1.2533/k_0$ for Case I, $L_f=1/k_0$ for Case II. The one-point velocity correlations, (9) and (12), have very different curvatures at $\tau=0$. (12) has negative loops for large decay time while (9) gives positive correlation for all τ. The integral time scale for $D(\tau)$ are: $T_{mE}=1.2533/\omega_0$ for I, $T_{mE}=0.5/\omega_0$ for II. The integral scales, T_{mE} and L_f, were set to the same value for the two cases so that results based on the two turbulences could be compared.

The simulated flow is governed by three parameters, i.e., u_0, T_{mE} (or ω_0), and L_f(or k_0). They are constant for a stationary (nondecaying) flow. If flow decays, they will change with time.

3 Programming Techniques

Some programming techniques used to ensure a successful simulation of the motion of heavy particles are discussed in this section. In our earlier paper (Wang and Stock, 1992), the equations of motion of a heavy particle

$$\frac{dv_i}{dt}=\frac{(u_i(y,t)-v_i)f}{\tau_a}+q\delta_{i3}, \tag{15}$$

$$\frac{dy_i}{dt}=v_i, \tag{16}$$

were numerically integrated by Hamming method, and the particle velocity, $v_i(t)$, and location, $y_i(t)$, were used to calculate the velocity correlations and mean square dispersions. Here q is the body force per unit mass, τ_a is the aerodynamic response time based on the Stokes drag. The factor f is the ratio of nonlinear drag coefficient to Stokes drag and is well represented for Reynolds number up to 1000 by the empirical relation (Rowe, 1961)

$$f=1+0.15\,\mathrm{Re}_p^{0.687}, \tag{17}$$

where Re_p is the particle Reynolds number. f/τ_a can be viewed as the drag force per unit mass per slip velocity acting on a moving particle.

When the drift parameter $\gamma=q\tau_a/u_0$ is large, the mean velocity of the particle in the vertical direction is much larger than the fluctuating velocity of the particle. Since the mean velocity was not known a priori, the computation of particle velocity correlations involved subtracting two large numbers, the mean square of particle velocity and the square of the mean velocity. The same situation is found when the mean square dispersion in the vertical direction is calculated. Therefore, for accurate results a very small time step size must be used.

To circumvent this difficulty, we can solve for the particle velocity relative to its drift velocity in still fluid v_{d0},

$$v_i'(t)=v_i(t)-\delta_{i3}v_{d0}. \tag{18}$$

v_{d0} is determined a priori from,

$$\frac{v_{d0}}{u_0}\left\{1+0.15\left[\frac{\rho d_p v_{d0}}{\mu}\right]^{0.687}\right\}=\gamma. \tag{19}$$

The drift velocity of a particle in the simulated turbulent flow is slightly larger than v_{d0} (Maxey, 1987), but the difference between the true drift and v_{d0} can be safely neglected (Wang and Stock, 1992). Therefore, the mean of $v_i'(t)$ should be close to zero. From (15) and (18), $v_i'(t)$ satisfies the following equation,

$$\frac{dv_i'(t)}{dt}=\frac{\{u_i(v_{d0}\delta_{i3}t+y_i'(t),t)-v_i'\}}{\tau_a}f(|u-v_{d0}\delta_{i3}-v'|)-\{v_{d0}f(|u-v_{d0}\delta_{i3}-v'|)+\gamma u_0\}\delta_{i3}/\tau_a. \tag{20}$$

The last term of (20) is very small due to Eq. (19). $y_i'(t)$ is the particle displacement relative to the mean location of particle in still fluid,

$$y_i'(t)=y_i(t)-\delta_{i3}v_{d0}t. \tag{21}$$

The relative displacement is given by

$$\frac{dy_i'(t)}{dt}=v_i'(t) \tag{22}$$

Now Eqs. (20) and (22) are solved simultaneously instead of (15) and (16). the Lagrangian velocity correlations and mean square dispersion are calculated from the relative velocity and relative displacement. This change avoids subtracting two large numbers and improves the accuracy of the results. Using the new set of equations, we found that, in the case of large particle drift velocity, the strict requirements for time-step size noted in the earlier paper (Wang and Stock, 1992) can be substantially relaxed.

A second improvement in the program was to numerically integrate Eqs. (20) and (22) for a sufficiently long time so that about 10 realizations of particle Lagrangian velocity correlations were obtained from each realization of the flow field. This technique can only be used for nondecaying flow and was found to reduce the effect of initial conditions on the results. Most of the results for nondecaying flow were obtained using 500 realizations of the random flow field with each realization providing 10 independent trajectories.

4 Scale Ratios in a Nondecaying Flow

4.1 The Continuity Effect. Particle dispersion coefficient is not isotropic due to the continuity effect, even if the carrying flow is isotropic and homogeneous. The particle dispersion coefficient in the horizontal direction (normal to the drift) is less than the particle dispersion coefficient in the vertical direction (parallel to the drift). For a large drift velocity, the ratio of the horizontal dispersion coefficient to the vertical dispersion coefficient approaches one half (Csanady, 1963). The particle rms fluctuation velocity (the velocity scale) and

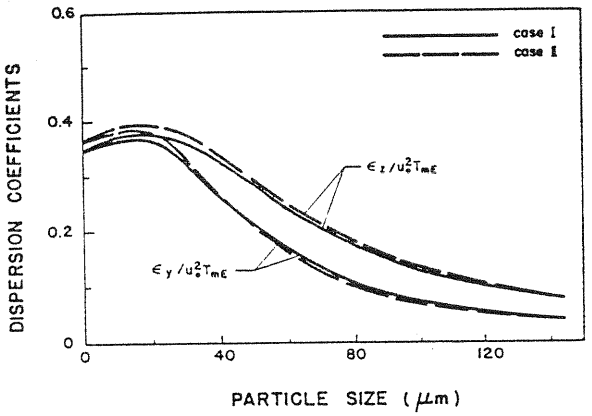

Fig. 3 Dispersion coefficients normalized by $\epsilon_0 = T_{mE} u_0^2$ as a function of particle size. ϵ_z is the dispersion coefficient in the vertical direction, and ϵ_y is the dispersion coefficient in the horizontal direction.

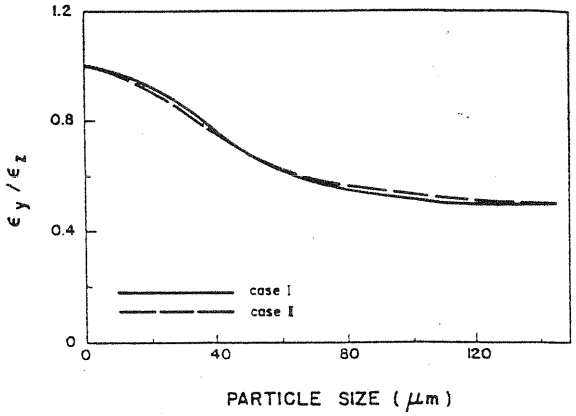

Fig. 4 Ratio of horizontal dispersion to vertical dispersion

the particle velocity-correlation time (the time scale) in the horizontal direction are also less than their respective values in the vertical direction (Reeks, 1977). Since the long-time dispersion coefficient is equal to the product of the velocity scale squared and the time scale, the diffusivity ratio, $\epsilon_{11}^p(\infty)/\epsilon_{33}^p(\infty)$, is related to the velocity scale ratio, v_{10}/v_{30}, and the time scale ratio, T_{11}/T_{33}, by

$$\frac{\epsilon_{11}^p(\infty)}{\epsilon_{33}^p(\infty)} = \left(\frac{v_{10}}{v_{30}}\right)^2 \times \frac{T_{11}}{T_{33}}, \tag{23}$$

where the subscript 1 (or 11) refers to the horizontal direction, and the subscript 3 (or 33) refers to the vertical direction.

Recently, Ferguson (1986) studied the continuity effect, using both numerical simulation and experimental measurements. His main consideration was the diffusivity ratio. His measurements showed the diffusivity ratio was close to one for 29 μm glass beads and the diffusivity ratio was close to a half for 62 μm glass beads. The experiment was not complete in the sense that the velocity scale ratio and time scale ratio were not considered. His simulation results verified the continuity effect on the diffusivity ratio and also showed that both the velocity scale ratio and time scale ratio were less than one. However, no comparison was made between his simulation and his measurements.

We can use numerical simulation to determine how the diffusivity ratio, the velocity scale ratio, and time scale ratio change with particle size for glass beads in grid-generated turbulence. In a real grid-generated turbulence, the flow scales change with time, so do the particle velocity scale and time scale. We postulate, however, that flow decay does not play a significant role in the scale ratios and diffusivity ratio. Based on this postulation, the scale ratios were simulated using a stationary (nondecaying) flow. Not considering flow decay in this section also facilitates the interpretation of results. To make possible a comparison between simulation results and Ferguson's experimental data, we used in the simulation the flow scales from the center of the test section in Ferguson's (1986) grid-generated turbulence. The flow scales were (see Appendix): $u_0 = 11.2$ cm/s, $T_{mE} = 0.225$ s, $L_f = 1.75$ cm. Both Case I turbulence and Case II turbulence were considered in this simulation.

4.2 Simulation Results. We consider the dispersion of glass beads ($\rho_p = 2600$ kg/m^3) in turbulent air under the normal gravity. The fluid viscosity is 1.8×10^{-5} kg/m·s and the fluid density is 1.14 kg/m^3. With the above flow scales, the Stokes number, drift parameter, and particle Reynolds number are given as a function of particle size in micrometers by,

$$\mathrm{St} = \tau_a / T_{mE} = 3.56 \times 10^{-5} d_p^2, \tag{24}$$

$$\gamma = \tau_a g / u_0 = 7.04 \times 10^{-4} d_p^2, \tag{25}$$

$$\mathrm{Re}_p = 7.1 \times 10^{-3} \left| \frac{u - v}{u_0} \right| d_p. \tag{26}$$

Figure 3 shows the simulation results for particle diffusivities, normalized by $T_{mE} u_0^2$, as a function of particle size. The long-time particle diffusivity was calculated from the mean square dispersion curves. When the particle size approaches zero, the heavy particles reduce to fluid elements and the normalized particle diffusivities are the same in both vertical and horizontal directions and equal to T_L/T_{mE}. T_L is the fluid Lagrangian correlation time. From Fig. 3, T_L/T_{mE} is 0.35 for Case I turbulence and 0.37 for Case II turbulence. The slight difference in T_L/T_{mE} between the two turbulences is due to the different shapes of fluid velocity correlations. The effect of the shape of fluid correlations on the particle dispersion coefficient tends to disappear as the particle size increases. The ratio T_L/T_{mE} for Case I turbulence is about the same as the value predicted by the second-order-iteration approximation (Wang and Stock, 1992).

Interestingly, the dispersion coefficients increase slightly with particle size when particle size is small. Since $T_{mE} > T_L$ in our simulation, the particle dispersion coefficient should increase with the inertia parameter in the absence of the drift (Reeks, 1977). On the other hand, the increase of the drift tends to reduce the particle dispersion coefficient due to the crossing trajectory effect. Because both the inertia and the drift increase with particle size, we have here the competing effects of inertia and drift on the particle dispersion coefficient. Our results imply that the inertia dominates the particle dispersion coefficient for the small size region. The dispersion coefficients reach maximum values at $d_p = 20$ μm, this is where the crossing trajectory effect offsets the inertia effect. Further increase in particle size causes rapid decrease in the particle diffusivities since the crossing trajectory effect controls the particle dispersion.

The diffusivity ratio is shown in Fig. 4. It decreases with particle size and approaches one half. The ratio is larger in Case I turbulence than in Case II for small particle size, but the opposite is true for large particle size. Nevertheless, the difference is very small. At $d_p = 62$ μm, our simulation predicts a ratio of 0.61 ± 0.03, which is in rough agreement with the measured value of 0.48 ± 0.11 (Ferguson, 1986).

The results for the time scale ratio and velocity scale ratio are more interesting (Fig. 5). The velocity scale ratio is very close to one for particle size up to 30 μm, which implies that particles respond to flow oscillations equally well in the horizontal direction as compared to the vertical direction for small particles. But as particle size goes beyond 40 μm, the velocity scale ratio drops very quickly with increasing particle size and reaches $1/\sqrt{2}$ for large particles. The time scale ratio decreases with particle diameter for small particles and has a minimum value at $d_p = 60$ μm. However, it increases with particle diameter for $d_p > 60$ μm and eventually returns to one.

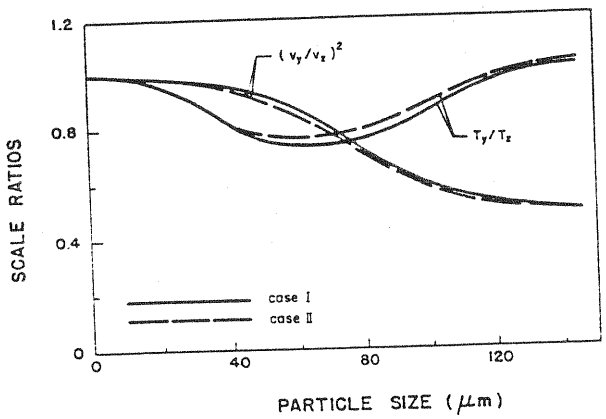

Fig. 5 Velocity scale ratio and time scale ratio

The two scale ratios, v_{10}^2/v_{30}^2 and T_{11}/T_{33}, determine the diffusivity ratio, according to Eq. (23). For small particle size, Fig. 5 shows that the time scale ratio governs the diffusivity ratio. Both the velocity scale ratio and the time scale ratio can affect the diffusivity ratio for intermediate particle size. As the particle size becomes large the reduction of the horizontal dispersion coefficient over the vertical dispersion coefficient is totally related to the difference in particle velocity scales in the two directions.

4.3 Discussions The motion of a heavy particle is governed by two time scales, the particle response time τ_a, which increases with the particle size, and the fluid correlation time in the neighborhood of the particle. The second scale can be direction-dependent. In the vertical direction it is related to the longitudinal fluid correlation and is roughly equal to L_f/v_d. L_f is the length scale of longitudinal spatial velocity correlation of fluid flow. However in the horizontal direction it is one half L_f/v_d, since the length scale for the transverse fluid correlation is one half L_f for a homogeneous and isotropic turbulence (Hinze, 1975).

Small particles ($\tau_a \ll L_f/v_d$) can respond quickly to fluid velocity fluctuations. The flow fluctuations have the same intensity in both direction because the flow is isotropic and homogeneous. Therefore, the particle velocity scale in the horizontal direction should be the same as that in the vertical direction. But, since the second time scale (fluid velocity time scale along the particle path) is direction-dependent, the particle time scale will be direction-dependent as well, as shown in Fig. 5. In summary, when particle size is small, the time scale ratio determines the diffusivity ratio.

For very large particles, we have $\tau_a \gg L_f/v_d$. The fluid velocity correlation time near the particle is very small compared to the particle response time. In this case, the particle motion resembles Brownian motion. The time scale of the particle is simply τ_a in all directions, i.e., the time scale ratio is one. Since the fluid velocity correlation time seen by the particle, the second time scale, in the horizontal direction is one half that in the vertical direction, the mean "frequency" of the random force acting on the particle due to the neighboring fluid in the horizontal direction is about twice the mean "frequency" in the vertical direction. Since the inertia is large, the particle can not respond to the fluid motion in the horizontal direction as to the same extent as in the vertical direction. Therefore, the particle velocity scale in the vertical direction is larger than that in the horizontal direction. More precisely, for very large particles

$$v_{10}^2 = u_0^2 \frac{L_f}{2 v_d \tau_a}, \quad v_{30}^2 = u_0^2 \frac{L_f}{v_d \tau_a}, \quad \frac{v_{10}}{v_{30}} = \frac{1}{\sqrt{2}}. \tag{27}$$

This is also shown in Fig. 5.

It is of interest to find the particle size for which the two scales, τ_a and L_f/v_d, are equal. The equality of the two time scales gives $\mathrm{St} \times \gamma = L_f/(u_0 T_{mE})$. For the particular flow used in this simulation, $u_0 = 11.2$ cm/s, $T_{mE} = 0.225$ s, and $L_f = 1.75$ cm, therefore, $\mathrm{St} \times \gamma = 0.694$. Using Eqs. (24) and (25), we find $d_p = 72$ μm. Therefore, if $d_p < 72$ μm, the time scale ratio mainly contributes to the diffusivity ratio; if $d_p > 72$ μm, the velocity scale ratio determines the diffusivity ratio. This same result can be seen in Fig. 5.

5 Comparisons With Experimental Data

5.1 The Grid-Generated Turbulence. Detailed experimental measurements of heavy particle dispersion in grid turbulence were made by Snyder and Lumley (SL 1971) and Wells and Stock (WS 1982). Both experiments used a grid with a mesh of spacing 2.54 cm. SL aligned their tunnel test section vertically; therefore, their measurements of dispersion in the plane perpendicular to the mean flow direction represent dispersion normal to the direction of the external force (horizontal dispersion). Their particles were released at $x/M = 20$, and they measured dispersion in the region from $x/M = 68.4$ to $x/M = 168$ where the flow decay rate is small. Here x is the distance from the grid and M is grid spacing. On the other hand, WS used a horizontal tunnel as a test section and they measured the dispersion of particles in the vertical direction. Their data represent particle dispersion in the direction of the drift velocity (vertical dispersion). The particles in WS's experiment were released at the grid, and they measured dispersion from $x/M = 20$ to $x/M = 70$ where the decay rate is large. They used charged particles and applied an electric field to control the particle drift velocity.

Grid-generated turbulence decays as (WS)

$$u'^2 \propto (x - x_0)^{-1}, \tag{28}$$

and the time scale grows as

$$T_{mE} \propto (x - x_0), \tag{29}$$

where x is the distance from the grid and x_0 is the virtual origin. The dispersion coefficient of fluid elements is almost independent of x since it is roughly proportional to $u_0^2 \times T_{mE}$. Because of this mutual balance of the turbulence energy and the time scale, the diffusion of fluid elements or small particles can be reasonably simulated with a stationary flow of scales matching at one point in the tunnel. However, the dispersion of heavy particles may be different from that of fluid elements. Using a direct numerical simulation, Ueda et al. (1983) found that the dispersion coefficient of heavy particles in decaying turbulence is not constant but rather decreases with time. The purpose of this section is to study the effect of the flow decay on the particle dispersion.

In what follows, the simulation results are compared with SL's and WS's data. Only the Case II turbulence is used for the following simulations because there is little effect of the shape of fluid velocity correlations on the particle dispersion.

5.2 Simulation Results Without Flow Decay. In this section the experiments of SL and WS are simulated using only one-point information for the flow scales and ignoring the flow decay. In simulating the particle dispersion of SL's experiment, the velocity scale and the spatial length scale were estimated based on Table 2 of SL's paper at $x/M = 73$: $u_0 = 13.1$ cm/s, $L_f = 3.1$ cm. Location $x/M = 73$ is about the center of the test section where the mean square dispersion was measured. No information on the integral time scale in the moving Eulerian frame, T_{mE}, was available. By matching the mean square dispersion curve for hollow glass beads from the simulation to the measured data, we obtained $T_{mE} = 410$ ms. This value of T_{mE} was then used to predict the dispersion and velocity correlation for other particles in the experiment.

Figure 6 shows the simulation results and experimental data for the mean square dispersion. The relative uncertainty for the mean square dispersion in the simulations was estimated

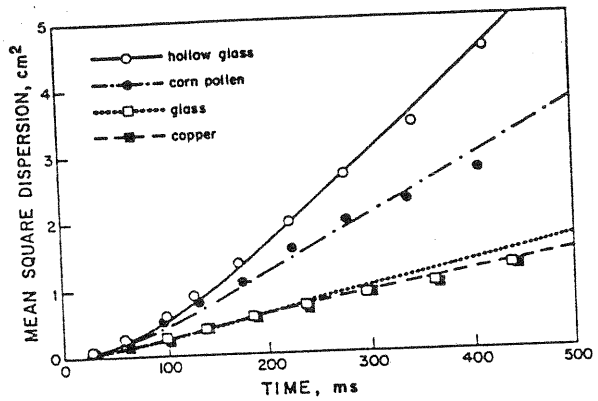

Fig. 6 Experimental and predicted mean square dispersions for the experiment of Snyder and Lumley. Flow decay is neglected in the simulation.

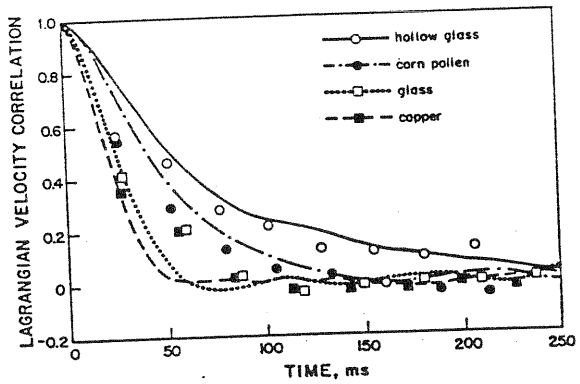

Fig. 7 Experimental and predicted Lagrangian velocity correlations for the experiment of Snyder and Lumley. Flow decay is neglected in the simulation.

to be 4 percent at a 95 percent confidence level. The simulated dispersion is in good agreement with the measured data. In particular, the slope for the mean square dispersion curve which is proportional to the dispersion coefficient is reasonably predicted. We note that for the glass and copper particles, the simulated dispersion coefficient is 10 – 20 percent larger. This may be partly due to the effect of flow decay, as discussed in the next section. The computed Lagrangian velocity correlation of the particle is compared to measured data in Fig. 7. The predicted shape of the correlations is fair but it is an improvement over the results of Ounis and Ahmadi (1989). The improvement is a result of using Case II turbulence.

The flow scales used to simulate WS's experiment were: $u_0 = 19.1$ cm/s, $T_{mE} = 122$ ms, and $L_f = 1.264$ cm. They were estimated using the flow details at $x/M = 30$ and matching the mean square dispersion for 5 μm particles with zero drift.

The simulated mean square dispersion for 5 μm particles with different falling velocities are shown in Fig. 8 along with the experimental data. The agreement between the simulated curves and the measured data is considered to be good. However, the agreement is not satisfactory for 57 μm particles (Fig. 9), particularly when the drift velocity is large. The predicted dispersion coefficient for 57 μm particles with 54.4 cm/s drift velocity is about 40 percent larger than the dispersion coefficient obtained from the mean slope of the measured dispersion data.

5.3 Inclusion of Flow Decay. In the last section, the numerically generated flow used in the simulation was stationary and the flow scales were constant. The flow decay in the streamwise direction of a grid-generated turbulence transforms into nonstationary of the flow in the moving Eulerian frame. The flow decay can be incorporated into the simulation by making the flow scales time-dependent. We shall only consider Wells

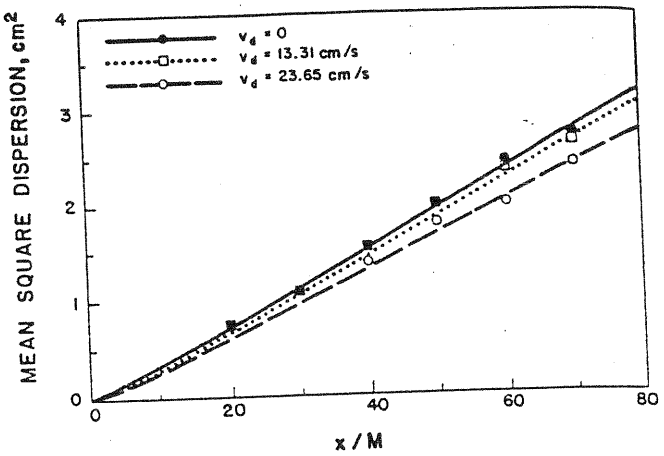

Fig. 8 Experimental and predicted mean square dispersions of 5 μm particles for the experiment of Wells and Stock. Flow decay is neglected in the simulation.

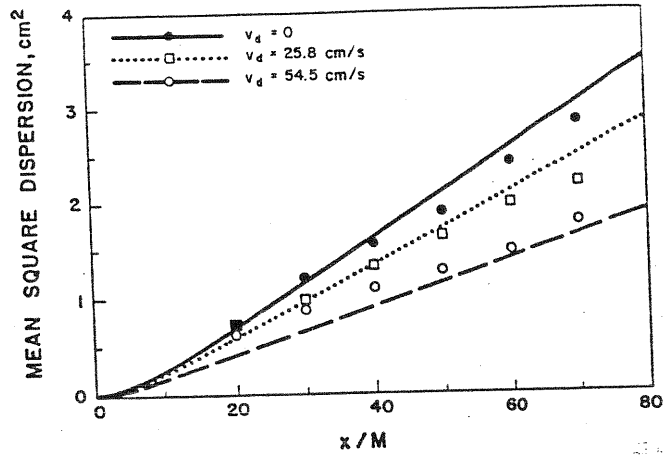

Fig. 9 Experimental and predicted mean square dispersions of 57 μm particles for the experiment of Wells and Stock. Flow decay is neglected in the simulation.

and Stock's (1983) experiment where the flow decay has a significant effect on the particle dispersion.

To include flow decay in the simulation, we need to know how the flow velocity scale and the flow time scale change with x/M. Using the flow scales at $x/M = 30$ and Eqs. (28) and (29) for WS's flow, we find

$$u_0 = 89.6\left(\frac{x}{M} - 7.987\right)^{-1/2} \text{ cm/s}, \tag{30}$$

$$T_{mE} = 1.39\left(\frac{x}{M} - 7.987\right) \text{ ms}. \tag{31}$$

The length scale is given by $L_f = T_{mE} u_0$, i.e.,

$$L_f = 0.125\left(\frac{x}{M} - 7.987\right)^{0.5} \text{ cm}. \tag{32}$$

The first point where the measurements of mean square dispersion were taken was $x/M = 20$. Before this point, the flow was very irregular. For convenience, we start the simulation at this location. Then the time in the simulation is related to the location in the tunnel by

$$t = \left(\frac{x}{M} - 20\right)\frac{M}{U}, \tag{33}$$

where the mean flow velocity U is 655 cm/s and the grid spacing M is 2.54 cm. Substituting (33) into (30)–(31), we obtain the flow scales required for the flow simulation,

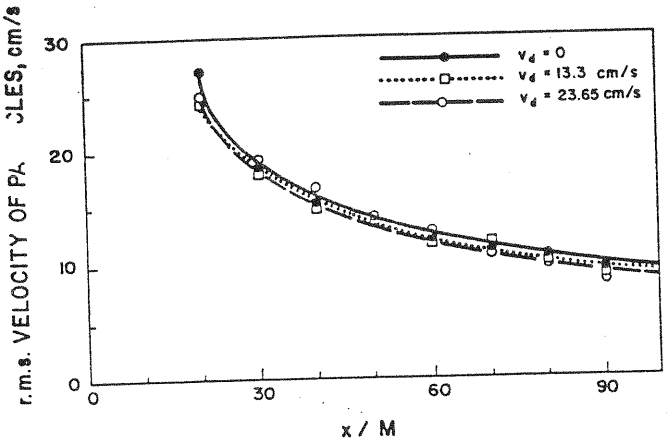

Fig. 10 Experimental and predicted RMS fluctuating particle velocities of 5 μm particles for the experiment of Wells and Stock. Flow decay is included in the simulation.

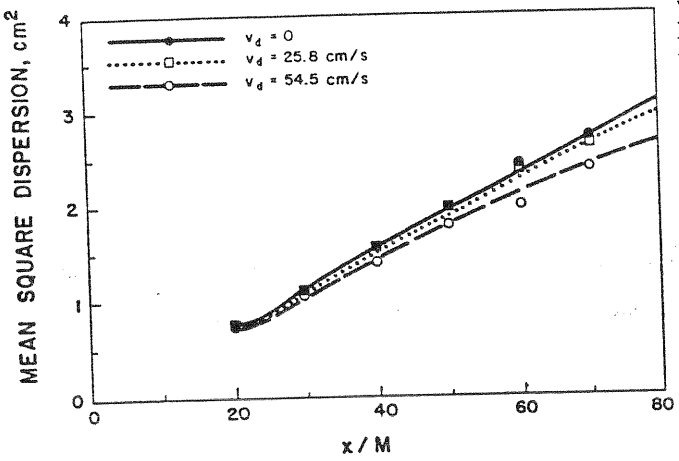

Fig. 11 Experimental and predicted mean square dispersions of 5 μm particles for the experiment of Wells and Stock. Flow decay is included in the simulation.

$$u_0(t) = 23.1(t+46.6)^{-1/2} \text{ cm/s}, \quad (34)$$

$$T_{mE}(t) = 0.358(t+46.6) \text{ ms}, \quad (35)$$

$$L_f(t) = 0.0635(t+46.6)^{0.5} \text{ cm}, \quad (36)$$

with t in ms. The flow was again simulated by Fourier modes as described in Section 2, using the modifications to the time-dependent scales given above.

The initial conditions for the particle were assumed to match the data at the first location, i.e., the initial location and the initial velocity were taken randomly with normal distributions of variances equal to the measured mean square dispersion and particle rms fluctuation velocity, respectively, at $x/M = 20$. The simulation results for $t > 0$ can then be compared to the measured mean square dispersion and rms velocity beyond $x/M = 20$. 3000 realizations of particle trajectories were used for the following results.

5.4 Simulation Results With Flow Decay. Figure 10 compares the predicted particle rms velocities with the measured data for 5 μm particles. The relative uncertainty for the simulated value of rms velocity is 3 percent at a 95 percent confidence level. For all three drift velocities, a good agreement is observed. As a result of the flow decay, the particles rms velocity decreases with the downstream location. The increase in the particle drift velocity tends to slightly reduce the particle rms velocity. The predicted mean square dispersions for 5 μm particles are shown in Fig. 11. They are in good agreement

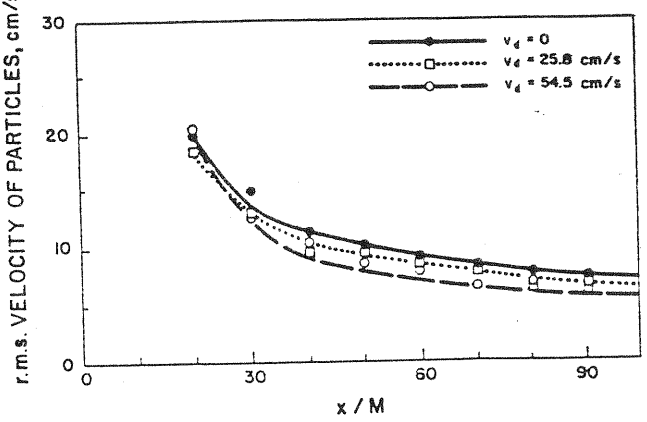

Fig. 12 Experimental and predicted RMS fluctuating particle velocities of 57 μm particles for the experiment of Wells and Stock. Flow decay is included in the simulation.

with the measured data. In addition, a small downward curvature for the largest drift case can be seen, indicating the local dispersion coefficient slowly decreases with distance down the tunnel.

The predicted particle rms velocities for 57 μm particles are shown in Fig. 12. The predicted particle rms fluctuation velocities are very close to the measured data. The dependence of the particle rms velocity on the drift velocity is clearly shown by the simulation. The particle velocity scale decreases with the drift, even though the inertia is kept the same. This decrease is caused by the fluid velocity correlation time in the neighborhood of the particle decreasing with the drift due to the effect of crossing trajectories, i.e., the "frequency" of the driving force is increased by the drift. In Fig. 12 we find a maximum of 25 percent difference in the rms fluctuation velocities between the largest drift particle and the zero-drift particle. Comparing Fig. 12 and Fig. 10, we see the rms velocity of 57 μm particles of zero drifts is about 25 percent less than that of 5 μm particles of zero drift. The 5 μm glass beads with zero drift follow closely the motion of fluid elements. Therefore, the reduction of the rms velocity for 57 μm particles with largest drift over that of fluid elements is half due to the particle inertia and half due to the particle drift. The effect of the drift on the particle velocity scale is substantially enhanced in this experimental work because of the artificial increase of the drift by an electric field.

The effect of flow decay on particle dispersion can be seen more obviously when the mean square dispersions of 57 μm particles are considered. Figure 13 shows the predicted curves and the measured data. For the largest drift case, the predicted curve of the mean square dispersion has an obvious downward curvature, i.e., the slope decreases with the downstream location. This indicates that particle dispersion coefficient decreases with time, as a result of the flow decay. WS (1983) simply calculated the dispersion coefficient based on the averaged slope of the measured dispersion data. The measurement of local dispersion coefficient is required in this case. The method used by Arnason and Stock (1984) might be used to make these measurements.

5.5 Explanation and Discussions. In general, particle dispersion coefficient in a given flow is controlled by the Stokes number (St) and the drift parameter (γ). St is a measure of the inertia and is defined as τ_a/T_{mE}. In grid-generated turbulence, St is related to x/M by

$$\text{St} = \frac{\tau_a}{1.39}(x/M - 7.987)^{-1}. \quad (37)$$

The effective particle inertia is reduced because of the increase of the flow time scale. For 57 μm particles ($\tau_a = 24.4$ ms), St

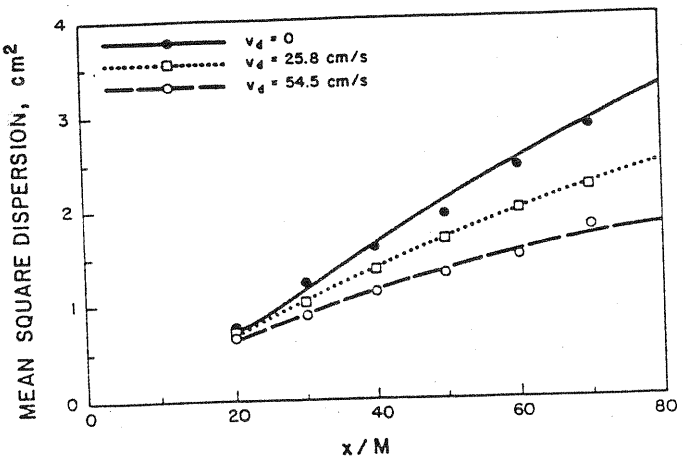

Fig. 13 Experimental and predicted mean square dispersions of 57 μm particles for the experiment of Wells and Stock. Flow decay is included in the simulation.

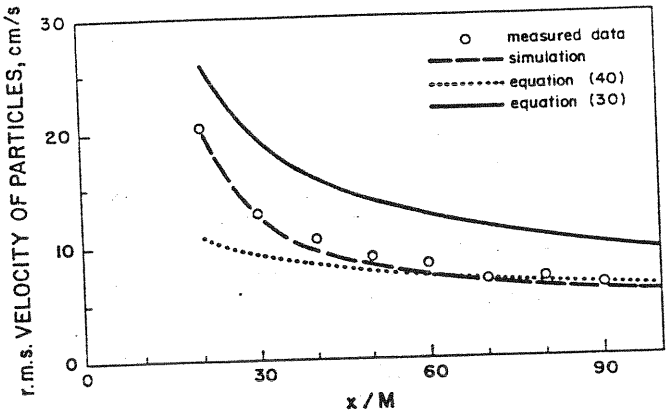

Fig. 14 The decay of the rms velocity for 57 μm particle of a drift velocity v_d = 54.5 cm/s, as compared to the asymptotic relation, Eq. (40), and the fluid rms velocity decay, Eq. (30)

is 1.46 at $x/M=20$ but reduces to 0.28 at $x/M=70$. On the other hand, the drift parameter defined as v_d/u_0 increases with the downstream location. Using Eq. (30), we have

$$\gamma=\frac{v_d}{89.6}(x/M-7.987)^{0.5}. \tag{38}$$

For the 57 μm particles with $v_d=54.5$ cm/s, γ is 2.1 at $x/M=20$ and increases to 4.79 at $x/M=70$. The drift parameter is much larger than the inertia parameter and the difference between γ and St grows quickly with x/M. As a result, particle dispersion is governed by the crossing trajectory effect and the local particle dispersion coefficient decreases with x/M, as shown by Fig. 13.

In the limit of large drift, the vertical particle dispersion coefficient is approximated by $u_0^2L_f/v_d$ (Yudine, 1959). Using Eqs. (30) and (32), we have

$$\epsilon_{33}^p\propto\left(\frac{x}{M}-7.987\right)^{-0.5}. \tag{39}$$

This approximation indicates that the local particle dispersion coefficient for particles of large drift decreases with distance at a -0.5 power in grid turbulence. Using Eqs. (27), (30), and (32), the vertical velocity scale for the 57 μm particles with a 54.5 cm/s drift is approximately equal to

$$v_{30}\approx 19.4\left(\frac{x}{M}-7.987\right)^{-0.25}, \tag{40}$$

which implies that the particle velocity scale decreases with distance from the virtual origin by a power of -0.25. This power is one half the power for the decay of fluid velocity scale (see Eq. (30)). Figure 14 compares the simulated particle rms velocity and the measured data to Eq. (30) and Eq. (40). Both the simulation and the measurements show better agreement with Eq. (40) for $x/M>50$. This suggests that the particle velocity scale has a slower decay rate than the fluid velocity scale, although the magnitude of the former is less due to particle inertia.

6 Summary and Conclusions

The aim of this study was to understand heavy particle dispersion by turbulence through a numerical simulation of particle motion in random velocity field generated by Fourier modes. We first extended the method for generating the flow to allow exponential fluid velocity correlations. Detailed numerical simulations were performed to study: 1) the anisotropic ratios of particle dispersion coefficient and scales; 2) the particle dispersion statistics in decaying grid-generated turbulences. Comparisons with the previous experimental data were made.

We found the time scale ratio decreases with particle size when the particle response time is less than the fluid velocity time scale in the neighborhood of the particle. It increases with particle size and returns to one when the particle size is large. The particle velocity scale ratio decreases monotonically with size and asymptotically reaches a value of $1/\sqrt{2}$. Therefore, for small particles, the particle time scale ratio determines the diffusivity ratio; but for large particles, the difference between the horizontal dispersion coefficient and the vertical dispersion coefficient is related to the difference between the particle velocity scale in the two directions. This result is embedded in the analysis of Reeks (1977) and partially shown in the simulation of Ferguson (1986). We expect the same scale-ratio behavior might be observed experimentally in isotropic wind tunnel flows.

Comparison of the simulation with the experimental measurements gives the following conclusions: 1) the simulation without flow decay can predict reasonable well the dispersion of heavy particles in a flow with slow decay (such as Snyder and Lumley, 1971); 2) for particle dispersion in faster decaying turbulence (such as Wells and Stock, 1983), the flow decay must be included in the simulation to predict the measured dispersion data; 3) the particle drift can reduce the particle rms velocity; 4) in a decaying flow, the local particle dispersion coefficient decreases with downstream location and the particle rms velocity decays slower than the fluid rms velocity.

The simulation indicates that the shape of fluid velocity correlations affects the shape of Lagrangian velocity correlation of the particle, but has little effect on the mean square dispersions, particle time scale and velocity scale.

This work was supported in part by funds of Summer Graduate Research Assistantship provided by Washington State University. The simulations were done on the University Computer Center's IBM 3090/300.

References

Arnason, G., and Stock, D. E., 1984, "Dispersion of Particles in Turbulent Pipe Flow," *Gas-Solid Flows*, J. T. Jurewicz, ed., FED-Vol. 10, pp. 25–29.

Csanady, G. T., 1963, "Turbulent Diffusion of Heavy Particles in the Atmosphere," *Journal of Atmospheric Science*, Vol. 20, pp. 201–208.

Calabrese, R. V., and Middleman, S., 1979, "The Dispersion of Discrete Particles in a Turbulent Fluid Flow," *American Institute of Chemical Engineers Journal*, Vol. 25, No. 6, pp. 1025–1035.

Ferguson, J. R., 1986, "The Effects of Fluid Continuity on the Turbulent Dispersion of Particles," Ph.D. dissertation, Washington State University.

Fung, J. C. H., Hunt, J. C. R., Malik, N. A., and Perkins, R. J., 1992, "Kinematic Simulation of Homogeneous Turbulence by Unsteady Random Fourier Modes," *Journal of Fluid Mechanics*, Vol. 236, pp. 281–318.

Gouesbet, G., Berlemont, A., and Picart, A., 1984, "Dispersion of Discrete Particles by Continuous Turbulent Motion. Extensive Discussion of the Tchen's Theory, Using a Two-Parameter Family of Lagrangian Correlation Functions," *Physics of Fluids*, Vol. 27, pp. 827–837.

Hinze, J. O., 1975, *Turbulence*, McGraw-Hill Book Co., New York.

Kraichman, R. H., 1970, "Diffusion by Random Velocity Fields," *Physics of Fluids*, Vol. 12, pp. 22–31.

Maxey, M. R., 1987, "The Gravitational Settling of Aerosol Particles in Homogeneous Turbulence and Random Flow Fields," *Journal of Fluid Mechanics*, Vol. 174, pp. 441–465.

Meek, C. C., and Jones, B. G., 1973, "Studies of the Behavior of Heavy Particles in a Turbulent Fluid Flow," *Journal of Atmospheric Science*, Vol. 30, pp. 239–244.

Mel, R., Adrain, R. J., and Hanratty, T. J., 1992, "Particle Dispersion in Isotropic Turbulence Under Stokes Drag and Basset Force with Gravitational Settling," *Journal of Fluid Mechanics*, Vol. 225, pp. 481–495.

Nir, A., and Pismen, L. M., 1979, "The Effect of a Steady Drift on the Dispersion of a Particle in Turbulent Fluid," *Journal of Fluid Mechanics*, Vol. 94, pp. 369–381.

Ounis, H., and Ahmadi, G., 1989, "Motions of Small Rigid Spheres in Simulated Random Velocity Field," *American Society of Civil Engineering Journal of Engineering Mechanics*, Vol. 115, pp. 2107–2121.

Pismen, L. M., and Nir, A., 1978, "On the Motion of Suspended Particles in Stationary Homogeneous Turbulence," *Journal of Fluid Mechanics*, Vol. 84, pp. 193–206.

Reeks, M. W., 1977, "On the Dispersion of Small Particles Suspended in an Isotropic Turbulent Field," *Journal of Fluid Mechanics*, Vol. 83, pp. 529–546.

Reeks, M. W., 1980, "Eulerian Direct Interaction Applied to the Statistical Motion of Particles in a Turbulent Fluid," *Journal of Fluid Mechanics*, Vol. 97, pp. 569–590.

Reeks, M. W., and McKee, S., 1984, "The Dispersive Effects of Basset History Forces on Particle Motion in a Turbulent Flow," *Physics of Fluids*, Vol. 27, pp. 1573–1582.

Riley, J. J., and Paterson, G. S., 1974, "Diffusion Experiments with Numerically Integrated Isotropic Turbulence," *Physics of Fluids*, Vol. 17, pp. 292–287.

Rowe, P. N., 1961, "The Drag Coefficient of a Sphere," *Transactions of Institute of Chemical Engineering*, Vol. 39, pp. 175–181.

Snyder, W. H., and Lumley, J. L., 1971, "Some Measurements of Particle Velocity Autocorrelation Functions in a Turbulent Flow," *Journal of Fluid Mechanics*, Vol. 48, pp. 41–71.

Squires, K. D., and Eaton, J. K., 1990, "Particle Response and Turbulence Modification in Isotropic Turbulence," *Physics of Fluids*, Vol. 2, pp. 1191–1203.

Townsend, A. A., 1976, *The Structure of Turbulent Shear Flow*, Cambridge University Press.

Turfus, C., and Hunt, J. C. R., 1979, "A Stochastic Analysis of the Displacements of Fluid Elements in Inhomogeneous Turbulence Using Kraichnan's Method of Random Modes," *Proceedings European Turbulence Conference*, Lyon.

Ueda, T., Jinno, K., Momii, K., and Maehama, K., 1983, "Numerical Study on the Diffusivity of Settling Particles in Homogeneous Isotropic Turbulence," *Transactions JSCE*, Vol. 15, pp. 293–296.

Wang, L. P., and Stock, D. E., 1988, "Theoretical Method for Obtaining Lagrangian Statistics from Measurable Eulerian Statistics for Homogeneous Turbulence," *Proceedings 11th Symposium on Turbulence*, Rolla, Missouri, B14.1–B14.12.

Wang, L. P., and Stock, D. E., 1992, "Numerical Simulation of Heavy Particle Dispersion-Time Step and Nonlinear Drag Considerations," ASME JOURNAL OF FLUIDS ENGINEERING, Vol. 114, pp. 100–106.

Wells, M. R., and Stock, D. E., 1983, "The Effects of Crossing Trajectories on the Dispersion of Particles in a Turbulent Flow," *Journal of Fluid Mechanics*, Vol. 136, pp. 31–62.

Yudine, M. I., 1959, "Physical Considerations on Heavy-Particle Dispersion," *Advances in Geophysics*, Vol. 6, pp. 185–191.

APPENDIX

Scale Estimation Based on the Flow of Ferguson (1986)

We report here how the parameters, u_0, T_{mE}, and L_f, were obtained from the information given in Ferguson (1986). They were estimated based on the flow of a mean velocity 4.5 m/s in Ferguson's experiment at $x/M=60$. The rms fluctuation velocity, u_0, was calculated from Eq. (4.7) of his dissertation, namely,

$$u_0 = 11.2 \text{ cm/s}. \tag{A.1}$$

The integral time scale, T_{mE}, was directly taken from Table 4.4 of his work,

$$T_{mE} = 0.225 \text{ s}. \tag{A.2}$$

T_{mE} was obtained based on the approximated relation, $T_{mE} = T_{fE}U/u_0$, where U is the mean flow velocity and T_{fE} is the Eulerian integral time measured at a fixed point $x/M=60$.

Since no direct information on the spatial length scale L_f was reported, we estimated it by examining Ferguson's data on thermal wake experiment. He found the dispersion coefficient of a thermal wake was about 15.5 cm^2/s with a different mean flow velocity of 6.7 m/s. In this flow, the velocity scale at $x/M=60$ was 16.8 cm/s (Eq. (4.8) of his dissertation) and $T_{mE}=0.182$ s. Then the Lagrangian scale $T_L = 15.5/(16.8)^2 = 0.055$ s. It follows that $T_L/T_{mE}=0.30$. According to Wang and Stock (1988), we have $2k_0T_{mE}u_0=4.2$ (Case I turbulence). This gives an estimated value for the wave number, $k_0 = 4.2/(2\times 0.182\times 16.08) = 0.718$ cm^{-1}. The spatial length scale associated with this k_0 is

$$L_f = 1.2533/k_0 = 1.75 \text{ cm}. \tag{A.3}$$

We assumed the length scale of the flow field with a mean velocity of 4.5 m/s at the same location was the same. This is a reasonable assumption since both flows were generated with the same grid (thus the same initial length scale) and in the same tunnel.